Molecular dynamics investigation of the stopping power of warm dense hydrogen for electrons

Yun Liu [1], Xing Liu [2], Shen Zhang,[3] Hao Liu [1,*] Chongjie Mo [4,†] Zhenguo Fu [5,‡] and Jiayu Dai[3]

[1]*Department of Applied Physics, School of Physics and Electronics, Hunan University, Changsha 410082, China*
[2]*Center for Applied Physics and Technology, School of Physics, Peking University, Beijing 100086, China*
[3]*Department of Physics, National University of Defense Technology, Changsha 410073, China*
[4]*Beijing Computational Science Research Center, Beijing 100193, China*
[5]*Institute of Applied Physics and Computational Mathematics, Beijing 100088, China*

A variety of theoretical models have been proposed to calculate the stopping power of charged particles in matter, which is a fundamental issue in many fields. However, the approximation adopted in these theories will be challenged under warm dense matter conditions. Molecular dynamics (MD) simulation is a good way to validate the effectiveness of these models. We investigate the stopping power of warm dense hydrogen for electrons with projectile energies ranging from 400–10000 eV by means of an electron force field (eFF) method, which can effectively avoid the Coulomb catastrophe in conventional MD calculations. It is found that the stopping power of warm dense hydrogen decreases with increasing temperature of the sample at those high projectile velocities. This phenomenon could be explained by the effect of electronic structure dominated by bound electrons, which is further explicated by a modified random phase approximation (RPA) model based on local density approximation proper to inhomogeneous media. Most of the models extensively accepted by the plasma community, e.g., Landau-Spitzer model, Brown-Preston-Singleton model and RPA model, cannot well address the effect caused by bound electrons so that their predictions of stopping power contradict our result. Therefore, the eFF simulations of this paper reveals the important role played by the bound electrons on stopping power in warm dense plasmas.

I. INTRODUCTION

The stopping power for charged particles in matter is a fundamental problem in numerous pivotal fields, such as medical radiation therapy [1–3], space exploration [4], astrophysics [5,6], DNA damage [7–9], and inertial confinement fusion (ICF) [10–13]. The energy deposition behavior of the hot electrons in the dense target is the key physical process in the fast ignition scheme of ICF. Considering that the warm dense matter (WDM) state is a typical state of materials in ICF [14–20], it is of great significance to study the energy deposition process of hot electrons in warm dense hydrogen [21–24].

A series of theoretical works have been carried out to explore the influence of various physical effects on the stopping power for charged particles under different conditions. The development of theoretical models of stopping power can be divided into two categories: one is the model developed based on collision concept, such as Landau-Spitzer (LS) model [25,26] and Li-Petrasso model (LP) [23], which is suitable for the thermal and fully ionized plasmas where collisions between particles are weak and dominated by the small angle scattering process. The other is based on the dielectric response function of the plasma to the charged particles like random phase approximation (RPA) model [27–29]. Recently, there are also models that combine the two-body collision and dielectric response, such as Brown, Preston, and Singleton (BPS) [30] model, in which the Lenard-Balescu kinetic equation and Boltzmann equation of pure Coulomb scattering are used to describe the long-distance collective excitation and short-distance hard collision of the plasma, respectively. However, different theoretical models have different ranges of applications. Considering the complexity of the warm dense state, the applicability of various theoretical models under the warm dense state needs to be verified by experiments or numerical simulation methods.

The previous experimental works on the stopping power for charged particles mainly focus on the incidence of ion beams in solids [31–33] and plasmas [34–38]. The time-of-flight (TOF) method with a semiconductor detector [39] is widely used for the measurement of the stopping power for the charged projectiles. However, only a few preliminary experiments have been reported until recently that study the energy loss of electrons in a gaseous target [40,41]. For instance, the mass stopping power for low-energy electrons traveling in gaseous H_2, which is unavailable straightforward in experiments, is obtained via intermediate measurements of electron energy loss spectra, which has to be artificially corrected for instrumental transmission effects [40]. So far, there is still a lack of accurate experimental data on the stopping power of warm dense plasmas for electron.

*haoliu@hnu.edu.cn
†cjmo@csrc.ac.cn
‡fu_zhenguo@iapcm.ac.cn

With the development of computational techniques, many kinds of numerical simulation methods have been proposed to improve the calculation of interactions of charged particles with matter, including time-dependent density functional theory (TD-DFT) in a real-time form [42–48], particle-in-cell (PIC) [1,21,49,50] and molecular dynamics (MD) [51–53]. In the high-temperature region of WDM, conventional TD-DFT methods need to include a large number of occupied eigenstates, which may cause huge computational costs [43,47]. An orbital-free version of TD-DFT [43,47] may partially relive this difficulty since only charge density of the electrons is involved but it may give an inaccurate estimation to the electron density of unionized or partially ionized states due to lack of electronic shell structures [54], which will influence the prediction of the electronic stopping power. The PIC simulation describes the dynamics of macroparticles, which represent many real particles with one model particle, rather than that of real particles. The collision between macroparticles needs to be described by a specific model. Therefore, the effectiveness of the stopping power predicted by PIC depends on the accuracy of the selected collision model [55–57]. The dynamical collision process between real particles can be simulated by the MD method, which directly solves the Newtonian equations of molecular motion without taking other assumptions except for the interaction potential between particles. Nevertheless, Coulomb catastrophe will occur in the MD simulations when we employ a target that contains both ions and electrons in a classical Coulomb system. Therefore, the previous classical MD works [52,58] can only consider the stopping power in a purely classical repulsive Coulomb system (e.g., an electron gas target). A recently published work [59] confirmed that collisions between electrons and ions have a significant impact on the transport features of electrons and ions. Therefore, it is necessary to consider the combined effect of ions and electrons in the system for the investigation of stopping power.

Compared with the classical Coulomb potential, the electron force field (eFF) potential can not only consider the entire contribution of electrons and ions in the sample plasmas to the stopping power, but also address the effects of electronic-structure-related processes, such as molecular dissociation, electronic excitation, and ionization. The eFF method is a further development of the wave-packet molecular dynamics (WPMD) [60], which is actually a widely accepted simulation method in the field of the warm dense plasmas. Many representative works using the eFF method can show the effectiveness of this method in dealing with the problem of warm dense matter [61]. The eFF method is excellent for practical nonadiabatic electron dynamics simulations of materials under extreme conditions and gave an excellent description of the shock thermodynamics of hydrogen from molecules to atoms to plasma [62], as well as the electron dynamics of the Auger decay in diamondoids following core electron ionization [63]. In addition, eFF was successfully applied to nonadiabatic processes such as dynamic shock Hugoniot [64], and exoelectron emission due to fracture in silicon [65]. Qian Ma *et al.* [66] investigated temperature relaxation with the method of eFF where the quantum effects of electronic degeneracy, delocalization, and quantum collisions are described naturally. The temperature-relaxation rates obtained by eFF agree with the experimental results. Therefore, the eFF method is suitable for the study of the stopping power of warm dense matter to charged particles.

A systematical investigation of stopping power for electrons in warm dense hydrogen was conducted with nonequilibrium molecular dynamics simulations using eFF potential in this work. At the investigated projectile-energy ranges from 400–10000 eV, it is shown that the stopping power decreases with increasing temperature of the sample, which contradicts the prediction given by most of the models extensively accepted by the plasma community. Meanwhile, the stopping power curves are found to be insensitive to the variation of temperature when the sample temperature is relatively low ($T < 1$ eV), which may be related to the molecular structure under low-temperature condition. Besides, the stopping power process of projectile electrons with low energy is also discussed in Appendix A. It is found that some low-energy ($E_0 < 100$ eV) projectile electrons may be trapped in the Coulomb field of the ions when the speed of the electrons is lower than the capture velocity of the potential field, which implies that the attraction potential of the ion to the electron will make the electron scattering trajectory exhibit completely different characteristics from that in a pure repulsive system.

The rest of this paper is organized as follows. The computational details of eFF simulation and the other theoretical models are introduced in Sec. II. Section III discusses the results of our simulation and Sec. IV concludes the entire work with a short summary.

II. COMPUTATIONAL DETAILS

A. eFF method

All eFF simulations in this work are performed using the eFF implementation included in the MD code LAMMPS [67]. The eFF method describes ions as classical charged particles and electrons as floating Gaussian wave packets by simplifying the electronic wave function to the form of

$$\Psi(\mathbf{r}) \propto \exp\left\{-\left[\frac{1}{s^2} - \frac{2p_s}{s}\frac{i}{\hbar}\right](\mathbf{r} - \mathbf{x})^2 - \frac{i}{\hbar}\mathbf{p_x} \cdot \mathbf{r}\right\}, \quad (1)$$

where s represents the size of wave packets, $\mathbf{x}$ is the center position of the wave packet, and p_s and $\mathbf{p_x}$ are corresponding momenta of s and $\mathbf{x}$. The equation of motion in eFF could be derived by substituting Eq. (1) into the time-dependent Schrödinger equation. Due to the simplification of electronic wave function, the eFF method makes it possible to simulate the dynamics of large-scale quantum systems.

A problem of the current eFF model is that the size of wave packet will be overspreading at high temperature [52], which weakens the scattering cross section of the electron. To avoid the wave packet spreading problem of projectile electrons, the constrained eFF (CEFF) method [66,68] is applied on the projectile electrons. When the size of the Gaussian wave packet for an electron is larger than its de Broglie wavelength, CEFF will impose a harmonic constraint on the motion equation of s to prevent further expansion of such wave packet. The comparison of the energy relaxation rate shows that the results predicted by CEFF are more consistent with the experimental
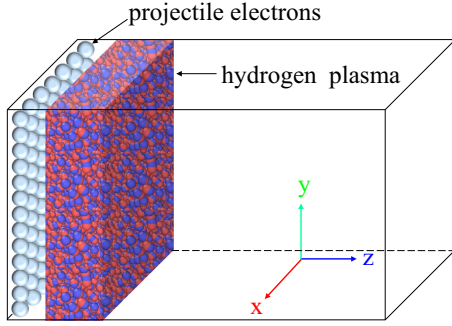
FIG. 1. The schematic diagram of the setup for eFF simulations.

results compared with the results of other theoretical models, which further proves the effectiveness of this scheme.

A scheme similar to the TOF method in experiments is used to simulate the stopping power problem in this work, which is different from the scheme used in the previous works [52,58]. In the previous MD simulations, the projectile particles moved in a periodic system and stayed in the sample throughout the whole simulation process. When counting the energy loss of an projectile electron, the electron may be accelerating or decelerating in the Coulomb potential field of the target particle, so the calculated energy loss cannot be considered as the final energy loss of the particle. Only when the projectiles penetrate through the sample and do not interact with the sample particles, the calculated stopping power can not be affected by the potential field of the sample, as measured by the experiments.

In order to eliminate the influence of the potential field of the sample on the results, a sample with a finite thickness is selected in our simulations, and a long flight distance is set after the sample, as illustrated in Fig. 1. The energy loss of the projectile is calculated when the particles penetrate through the sample and moves far away from the sample so that the stopping power obtained can be independent of the potential of sample. However, the limited thickness of the sample brings about the problem of boundary effects, which does not exist in the periodic system. Considering that the boundary effect is only significant in a thin layer near the boundary, whose characteristic thickness is of the order of mean interatomic distance, the influence of the boundary effect on the result can be ignored when the thickness of the entire sample is much larger than the thickness of the boundary layer. Meanwhile, the thickness of the sample should not be too large to ensure that most of the projectiles can penetrate through the sample. The Wigner-Seitz radius of hydrogen atoms is $r_s = 3.1722$ bohr in our simulation, corresponding to a density of solid hydrogen $\rho = 0.085$ g/cm^3. Therefore, the thickness of the entire sample is set to 102 bohr, which is more than 30 times of r_s.

The simulation box has a size of 255 bohr $(x) \times 255$ bohr $(y) \times 1530$ bohr (z) and the sample plasmas are confined in a thin region ($0 < z < 102$ bohr) with two reflecting wall. Periodic boundary conditions are adopted along the x and y directions, and two reflecting wall are used for all particles at both ends of the z axis to prevent particles from escaping the simulation box. The sample hydrogen plasma contains 50000 protons and 50000 electrons, and the masses of protons

and electrons are set to $m_i = 1.00794$ amu and $m_e = 0.00055$ amu, respectively. The cutoff radius of the interaction potential in the simulations is set as $r_{\rm cut} = 15$ bohr, which is about five times of the r_s and large enough to ensure the convergence of the calculation results.

The initial configuration of target plasma uses a simple cubic lattice to uniformly place hydrogen molecules in the sample area. Each hydrogen molecule is composed of two hydrogen nuclei and two electrons with opposite spins. The initial distance between the two hydrogen nuclei is set to 1 bohr, and the initial position of the two electrons is the midpoint of the line connecting the two hydrogen nuclei. The initial value of s and p_s for all target electrons are set as 1 bohr and 0 bohr/fs, respectively. In order to achieve the thermodynamic equilibrium of the system at the target temperature we set, the ion temperature in the target was controlled with a rescale method. The electron temperature will reach equilibrium through the energy relaxation between the electron and the ion.

The stopping power of the target for each projectile electron can be calculated as

$$-\frac{dE_i}{dx} \approx -\frac{\Delta E_i}{\Delta z} = \frac{E_{iz}(0) - E_{iz}(t)}{\Delta z}, \qquad (2)$$

where E_{iz} is the component of kinetic energy of projectile electron with index i along axis z, $E_{iz}(t)$ and $E_{iz}(0)$ is the final and initial value of E_{iz}, and Δz is the thickness of the target. The mean stopping power $-\overline{dE/dx}$ of the target can be obtained by the statistical average of a large number of the stopping power of projectile electrons.

In order to save computational resources, each simulation contains 100 projectile electrons. Initially, 100 electrons are distributed in the area of $z \in [-2, 0]$ bohr and two reflective walls are used to confine them in this area. The mean distance between two projectile electrons is about 25 bohr and the interaction between these electrons is very weak, so the difference between the result obtained in our simulations and that obtained in the case with single projectile electron is very small. After the sample plasma reaches the thermodynamic equilibrium condition, an initial velocity is applied to all the projectile electrons and the reflective constraint on them is removed, so that the projectile electrons can inject into the sample plasmas. In addition, for samples with the same state, we have performed several repeated calculations using different random number seeds for the initial velocity distribution, to ensure that the uncertainty of the average stopping power obtained is within an acceptable range.

The temperature of target plasma is set to be 0.1 eV, 0.4 eV, 1 eV, 2 eV, 4 eV, and 10 eV and the corresponding plasma parameters are listed in Table I. The coupling parameter Γ_{ee} corresponds to the ratio of the interaction potential energy to the thermal energy and the definition expression can be written as [69]

$$\Gamma_{ee} = \frac{e^2}{a_e \sqrt{(k_B T)^2 + E_F^2}}, \qquad (3)$$

where $a_e = (\frac{4\pi n_e}{3})^{-1/3}$ is the Wigner-Seitz radius of the electrons in the target, $E_F = \frac{\hbar^2}{2m_e}(3\pi^2 n)^{2/3}$ is the Fermi energy, in which n is the electron number density. The value of Γ_{ee} in our

TABLE I. The value of coupling parameter Γ_{ee}, degeneracy parameter Θ, and WDM parameter W of the target plasmas with different target temperature.

T(eV)	Γ_{ee}	Θ	W
0.1	10.99	0.13	0.015
0.4	5.56	0.27	0.085
1	3.52	0.45	0.25
2	2.55	0.74	0.55
4	1.65	1.20	0.85
10	0.79	2.33	0.71

simulations ranges from 0.79–10.99, covering the range from weak coupling to strong coupling. The degeneracy parameter is defined as

$$\Theta = \frac{k_B T}{E_F}, \quad (4)$$

and the WDM parameter W of sample is defined as

$$W(T, p) = S(\Gamma_{ee})S(\Theta) \quad (5)$$

as the definition in Ref. [70], where $S(x) = \frac{2}{x+x^{-1}}$.

The energy range of projectile electrons is set from 400–10000 eV. When the speed of the projectiles is much greater than the thermal motion speed of the particles in the sample, the dynamic effect of the sample particles is not significant and the stopping power of the entire sample for projectiles is close to the effect of a static potential field, so the MD simulation is unnecessary. On the other hand, the projectile electrons cannot penetrate through the target if its initial energy is too small and the calculation of the stopping power cannot be preformed. To illustrate these situations, the dynamic features of projectile electrons with low speed (10 eV ∼ 100 eV) are discussed in Appendix A.

The cutoff radius for pair interactions is set to be 51 bohr, which is 15 times more than the Wigner-Seitz radius of hydrogen atoms and meets the requirement of convergence. Each simulation has a different and a relatively small time step $\Delta t = 10^{-5}$ fs $\sim 10^{-6}$ fs to ensure the quasicontinuity of the particle trajectory, especially at the moment of collision.

B. RPA model and LDA correction

In this work, the calculated stopping powers of eFF are compared with that of BPS model [30], RPA model as well as a corrected version of RPA model via local density approximation (LDA). The RPA model based on homogeneous electron gas at a fixed density gives the Lindhard electronic stopping power S_e^{RPA} [71] with the velocity v is expressed as

$$-\frac{dE}{dx}^{\text{RPA}}(v) = S_e^{\text{RPA}}(v)$$
$$= \frac{2Z^2}{\pi v^2} \int_0^\infty \frac{dq}{q} \int_0^{qv} d\omega \text{Im}[-\varepsilon^{-1}(q, \omega)], \quad (6)$$

where the charge number Z of the moving electron equals 1. The RPA dielectric function [71] emerging in Eq. (6) at

a given momentum/energy transfer q/ω is written as

$$\varepsilon(q, \omega) = 1 - \frac{1}{\pi^2 q^2} \int d\mathbf{k} \frac{f(\mathbf{p}+\mathbf{k}/2) - f(\mathbf{p}-\mathbf{k}/2)}{\mathbf{k} \cdot \mathbf{q} - \omega - i\eta}, \quad (7)$$

with the Fermi distribution function $f(\mathbf{k}) = 1/\{\exp[(k^2/2 - \mu)/T] + 1\}$, an infinitesimal number η, chemical potential μ, as well as the electronic temperature T. A local-density approximation (LDA) method [72] combined with RPA model is further introduced in order to evaluate the stopping power provided by core electrons for a projectile electron. This approximation assumes that the electronic stopping power of a real inhomogeneous material can be determined by the spatial average over the Lindhard electronic stopping power S_e^{RPA} evaluated at the local density $\rho(\mathbf{r})$, i.e.,

$$-\frac{dE}{dx}^{\text{LDA}}(v) = S_e^{\text{LDA}}(v) = \frac{1}{\Omega} \int_\Omega d\mathbf{r} S_e^{\text{RPA}}(\rho(\mathbf{r}), v) \quad (8)$$

with the volume Ω, and the position $\mathbf{r}$. With this approximation, the electronic stopping power contributed by the ultrahigh electronic density of core electrons near the nuclei can be qualitatively addressed.

The local densities $\rho(\mathbf{r})$ are provided by the finite-temperature density functional theory (FT-DFT) based on the ionic configurations extracted from first-principles molecular dynamics (FPMD) simulations after equilibrium. For higher temperatures ($T \geq 4$ eV), the extended FPMD (ext-FPMD) and DFT are adopted to overcome the difficulty of too many electronic states demanded by the traditional DFT method [73]. The FPMD and FT-DFT simulations are carried out using a revised QUANTUM ESPRESSO package [73,74], containing 64 ions in a cubic box with $\rho = 0.085$ g/cm^3. A canonical system of constant NVT is adopted with the time step of ionic motion varying from 0.15–1 fs depending on the temperature of the system. The projected augmented wave [75] pseudopotential is employed with a core cutoff radius $r_c = 0.9$ bohr. The Γ-point sampling of the Brillouin zone is used in the calculations, together with the exchange-correlation functional of Perdew, Burke, and Ernzerhof [76], and a plane wave cutoff energy of 70 Ry. 320 bands are explicitly included with the top 200 used to determine the effective potential energy [73]. After initial equilibrium, eight configurations are selected randomly for further FT-DFT calculation to obtain $\rho(\mathbf{r})$. To ensure the accuracy, a norm-conserving pseudopotential are used in the calculations with a cutoff radius of 0.6 bohr, and a plane wave cutoff energy of 80 Ry, as well as a $2 \times 2 \times 2$ shifted k-point mesh to resolve the Brillouin zone.

C. BPS model

The BPS method for the stopping power of weakly coupled plasma to charged particles is given by

$$\frac{dE}{dx} = \sum_b \left(\frac{dE_{b,S}}{dx} + \frac{dE_{b,R}^<}{dx} + \frac{dE_b^Q}{dx} \right). \quad (9)$$

The first term $\frac{dE_{b,S}}{dx}$ represents the classical short-distance hard collision contribution, which is derived from the Boltzmann equation. The second term $\frac{dE_{b,R}^<}{dx}$ is the classical long-distance collective excitation contribution, which is derived from the Lenard-Balescu kinetic equation. The third term $\frac{dE_b^Q}{dx}$ is the
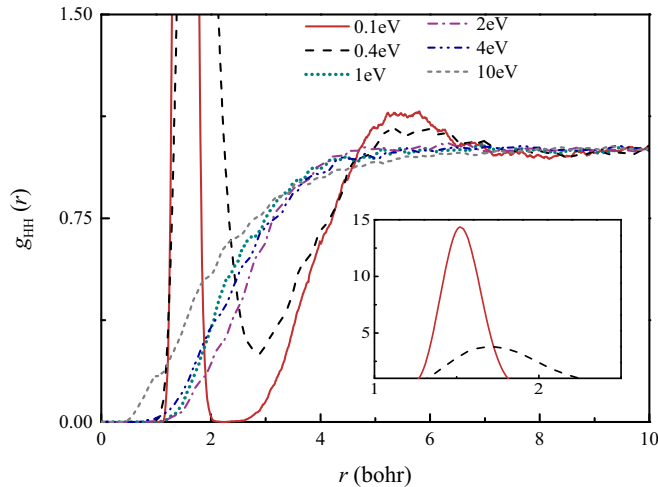
FIG. 2. Profiles of H-H RDF in warm dense hydrogen under different temperature. The inset is used to show the peak feature of the RDF corresponding to the hydrogen-hydrogen bond under low temperature conditions. The solid red line, the dashed black line, the short-dot dark-cyan line, the dash-dot purple line, the dash-dot-dot dark-blue line, and the short-dash gray line correspond to the case with the target temperature of 0.1 eV, 0.4 eV, 1 eV, 2 eV, 4 eV, and 10 eV, respectively.
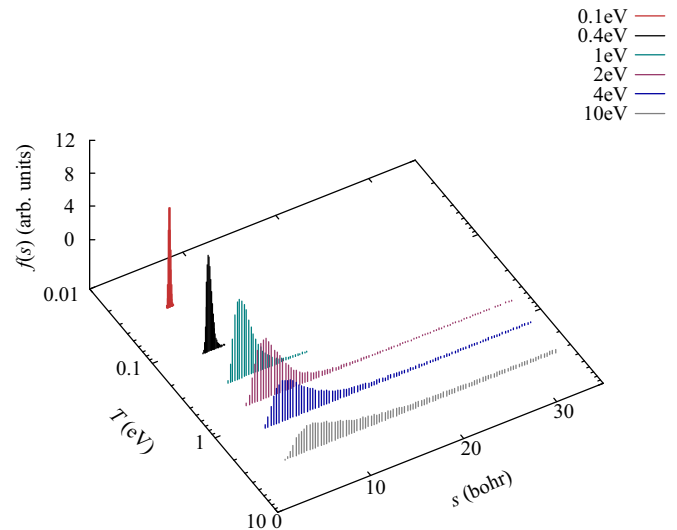

FIG. 3. The size distribution of electronic wave packet $f(s)$ in the target at varying temperature. From top to bottom are the red line, the black line, the dark-cyan line, the purple line, the dark-blue line, and the gray line, corresponding to the distribution under the target temperatures of 0.1 eV, 0.4 eV, 1 eV, 2 eV, 4 eV, 10 eV, respectively.

quantum correction to the classical part. The subscript b denotes the ions in the plasma. Detailed expressions for each term are clearly presented in Ref. [30], and thereby, we will not show them in this work for briefness. Here, we would like to point out that (i) in the BPS model, the electrons and ions are considered as classical particles, which obey the Maxwell-Boltzmann distribution; (ii) the quantum correction becomes significant when the quantum Debye wavelength becomes larger than the classical minimum approaching distance; and (iii) the BPS model is only suitable for the weakly coupled plasmas.

III. RESULTS AND DISCUSSIONS

The stopping power of warm dense hydrogen for projectile electrons is investigated at a same density of solid H_2, but different temperatures to cover a wide range of coupling parameters of WDM. Before discussing the stopping power, it is necessary to analyze the electronic and ionic structures of hydrogen targets in the simulated conditions, which, shown as follows, will significantly affect the later estimations of stopping powers. Here, the radial distribution function (RDF) of hydrogen ions $g_{HH}(r)$ and the size distribution function of target electronic wave packets $f(s)$ are illustrated, respectively, in Figs. 2 and 3 in order to qualitatively describe the degree of molecular dissociation and electronic excitation in the sample plasma at different temperature.

As shown in Fig. 2, the peak structure near $r = 1.5$ bohr of $g_{HH}(r)$ corresponds to the bond length of hydrogen molecules and the height of this peak can qualitatively reflect the dissociation degree of hydrogen molecules in the system. It is found that the height of the peak in RDF decreases as the sample temperature increases. The height of the peak of hydrogen molecule is very large in the sample at $T = 0.1$ eV, indicating

a low degree of molecular dissociation. When the sample temperature is higher than 1 eV, the peak of molecular feature disappears on the curve of RDF, indicating that the hydrogen molecules are completely dissociated.

The distribution of the target electronic wave packet sizes in Fig. 3 shows that the sizes of the electrons is mostly confined inside the average intermolecular distance at low system temperatures ($T < 1$ eV), indicating that most of the electrons occupy localized states. As the temperature of the sample increases, the sizes of the electron wave packets show a broadening trend, indicating that more and more target electrons are in excited states.

The calculated stopping power of hydrogen plasmas at solid density and different temperatures are shown in Fig. 4. First of all, it can be seen that, at any simulated temperature, the value of stopping power $-\overline{dE/dx}$ shows a monotonous decrease as the increase of projectile electron energy from 400–10000 eV. This phenomenon shows qualitative agreement with experiment carried out by Munoz *et al.* [41], where the stopping power of H_2 to projectile electron is measured at incident energies from 50–5000 eV and the maximum value of stopping power is found at the projectile energy of about 100 eV. In addition, the stopping power predicted by various theoretical models in the projectile energy range of 400–10000 eV also shows that the stopping power decreases monotonously with respect to the projectile energy, as illustrated in Fig. 5. That is to say, the monotonous trends predicted by the eFF method are consistent with the results obtained by both experiments and theoretical models. The reason for this trend can be explained as, the scattering angle of the collision between projectile electrons and target particles decreases and the scattering cross section becomes smaller, as the projectile energy increases, so that the momentum transfer in the collision process becomes smaller.
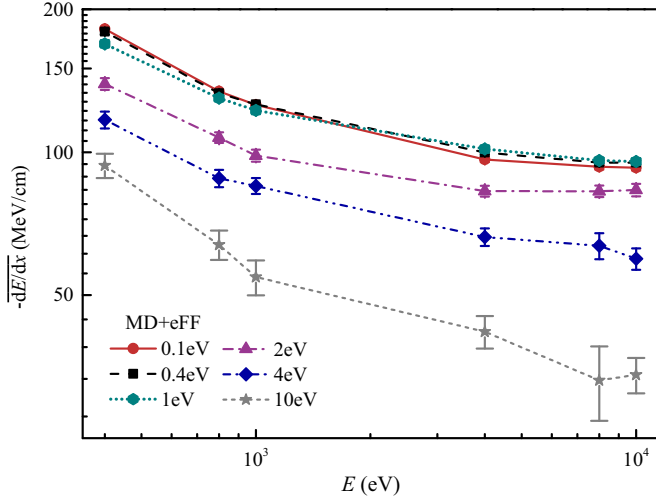
FIG. 4. The mean stopping power $-\overline{dE/dx}$ of warm dense hydrogen to electrons as a function of projectile electron energy. The solid red line with solid circle points, the black dashed line with square points, the dark-cyan short-dot line with hexagon points, the purple dash-dot line with triangle points, the dark-blue dash-dot-dot line with rhombus points, and the gray dashed line with five-pointed star points correspond to the case with the target temperature of 0.1 eV, 0.4 eV, 1 eV, 2 eV, 4 eV, and 10 eV, respectively.

The effect of sample temperature on stopping power is also explicitly displayed in Fig. 4. It is found that, at relatively low temperatures in the range of 0.1–1 eV, the stopping power is not sensitive to the variation of temperature. However, with plasma temperature further increasing from 1–10 eV, there is a noticeable reduction in the stopping power, which means that the temperature becomes a major factor. These two findings provided by eFF simulations contradict the predictions given by most of the other theoretical models broadly used for
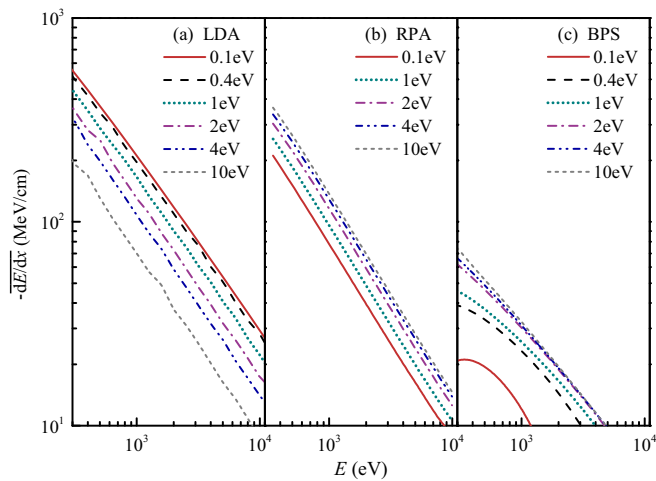

FIG. 5. The stopping power of warm dense hydrogen obtained with (a) LDA corrected RPA calculation, (b) RPA model, and (c) BPS model. The solid red line, the dashed black line, the short-dot dark-cyan line, the dash-dot purple line, the dash-dot-dot dark-blue line, and the short-dashed gray line correspond to the case with target temperature of 0.1 eV, 0.4 eV, 1 eV, 2 eV, 4 eV, and 10 eV, respectively.

weakly coupled plasmas starting from homogenous systems. Particularly, we present the calculated results of stopping power via the BPS model and the one-component RPA model in the same conditions, as shown in the Figs. 5(b) and 5(c). In each model, the projectile electron is treated as a classical negative point charge and the hydrogen target is assumed to be fully ionized. It is clearly shown that, in both of BPS and RPA models, the stopping power increases with the sample temperature increasing, which is contrary to the results obtained by our eFF simulations.

Under different sample plasma temperatures, the scattering cross section during particle collision will be different, which will eventually affect the stopping power. The collision scattering cross section of the sample electron to the projectile electron can be affected by two factors, one is the strength of the interaction between the two particles, and the other is the relative velocity of the two particles. (i) When the relative velocity of two particles is the same, the stronger the interaction potential, the larger the scattering cross section. (ii) When the interaction potential is determined, the greater the relative velocity of the two particles, the smaller the scattering cross section. This is why the stopping power decreases monotonously with the increase of projectile energy.

Here, we will discuss how the temperature affects these two factors in the eFF simulations, thereby affecting the collision scattering cross section. Under the description of the eFF method, the interaction potential energy between two electrons is in the form of

$$V_{ee} = \frac{1}{4\pi\varepsilon_0} \sum_{i \neq j} \frac{1}{r_{ij}} Erf\left(\frac{\sqrt{2}r_{ij}}{\sqrt{s_i^2 + s_j^2}}\right), \qquad (10)$$

where r_{ij} is the distance between two electrons, and s_i and s_j are the wave packet size of the two electrons. As the temperature of the system increases, the mean size of the sample electronic wave packet becomes larger and the interaction between the projectile and target electron becomes weaker, which will reduce the scattering cross section and lead to a decrease in stopping power.

At the same time, the increase in the sample temperature will also increase the mean relative velocity in the collision, thereby reducing the scattering cross section. However, we note that according to the plasma theory, the rise of temperature mainly reduces the plasma collision cross section of the sample rather than the collisional cross section between the projectile and the target. Since the energy of the projectile is much larger than the kinetic energy of the sample particle in our eFF simulations, the increased temperature of the target we consider here has a negligible effect on the relative collision velocity between the projectiles and target electrons.

Above all, the difference in the target electron wave packet size distribution at different sample temperatures results in a different strength of the interaction potential, which makes the stopping power show a negative correlation with temperature in our eFF simulations. A recently published work [77] proposed a theoretical model to calculate the stopping power for protons propagating through plasmas. The result predicted by this model shows that the stopping power will decrease as
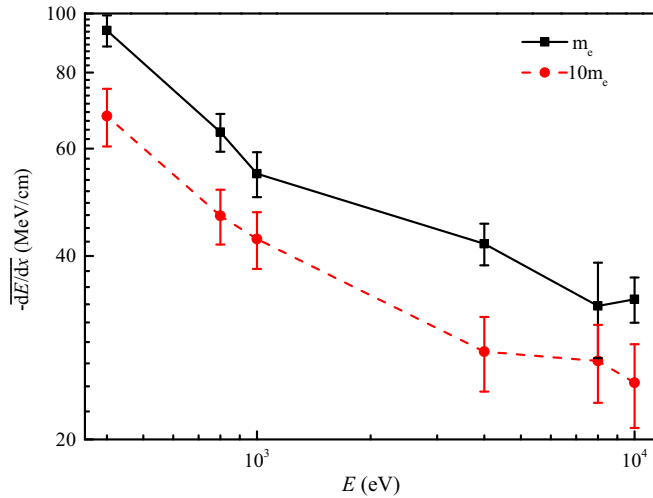
FIG. 6. The mean stopping power curve of the target to electrons at a target temperature of 10 eV, where the electronic masses in simulations are set to 0.00055 amu (real electron mass m_e, represented with the black solid line with square points) and 0.0055 amu (ten times real electron mass $10m_e$, represented with the red dash line with circle points), respectively.

the target temperature increases, which is consistent with our result obtained with eFF.

The next phenomenon that needs to be explained is why the stopping power curves do not change significantly with temperature when the sample temperature is in the range of 0.1–1 eV. As mentioned earlier, the interaction between projectile electrons and target electrons will increase due to the smaller wave packet size of the target electrons, as the target temperature decreases. However, the interaction between the electrons and ions in the sample will also be enhanced at the same time, and a stable molecular structure will be formed under the low temperature, as shown in Fig. 2. The corresponding physical picture is that the target electrons are tightly bound to the ions, which is equivalent to increasing the effective mass of the target electrons during the collisions. When a light high-speed particle collides with a heavy particle, the light particle will bounce away with almost no loss of kinetic energy. The final result is that the amount of energy transferred from the light particle to the heavy particle during the collision will be very small. This is why the stopping power contributed by ions in the sample is much smaller than the contribution of electrons. Therefore, as the sample temperature decreases, the energy transfer efficiency of each effective collision between the projectile electron and the target electron will decrease due to the increase in the equivalent mass of the target electron, which ultimately leads to a decrease in the stopping power of the target.

In order to verify the influence of electron mass on stopping power, we calculated the stopping power of hydrogen plasma with electron mass ten times the real electron mass, and the other conditions are the same as the case with a sample temperature of 10 eV, as illustrated in Fig. 6. It can be found that the stopping power of the sample with heavier electrons is significantly lower than that of the sample with

lighter electrons, which proves that the electron mass in the sample can significantly affect the value of stopping power.

The competitive balance of these two mechanisms makes the change of stopping power with temperature in the low-temperature range insignificant. As the temperature further rises beyond 1 eV, the electrons break free from the bondage of the ion so that the balance is broken and the temperature dependence of the stopping power appears.

In addition, the BPS model is only suitable to the weakly coupled plasmas. The coupling parameter of warm dense H considered in this work ranges from 0.57–57, which means most of the plasma states considered here are beyond the scope of application of the BPS model. This may also be a reason for the significant difference between the results of the BPS model and the eFF simulations. On the other hand, the interaction between particles and the correlation effect between electrons and ions are ignored in the one-component RPA model. These effects are critical physics properties of WDM, which determine the transport properties and the energy deposition mechanism of charged particles in WDM. However, a modified interaction potential in Eq. (10) is employed in the eFF method, which could partially consider these special properties of WDM. Therefore, the difference between the results of the RPA model and the eFF simulation may be understandable. This also indicates that the bound electrons in WDM play important roles on the energy deposition of charged projectiles.

In summary, in the eFF simulation, sample temperature affects the strength of the interaction between electrons and electrons, or that between electrons and ions, through changing the electronic structure and molecular structure of the target, thereby determining the target's stopping power to electrons. Both RPA and BPS models do not include the inhomogeneous effects of electronic structure, so their calculated stopping power and the calculation of the eFF method show different trends.

In order to further evaluate the effect of electronic structure on stopping power provided by bound states, we thus introduce a correction of local-density approximation (LDA) [72] to the Lindhard electronic stopping power model based on RPA dielectric response [71]. This approximation assumes that the electronic stopping power of a real material can be determined by the spatial average over the RPA stopping power of homogenous electron gas evaluated at the microlocal density, so that the electronic structure of bound states is roughly introduced through inhomogeneous electron-density distribution obtained by DFT calculations with the LDA exchange-correlation functional. This LDA method merely gives a qualitative prediction to the contribution of bound electrons to the stopping power since it always overestimates this contribution compared with a more precise TD-DFT method [72]. The calculated result of the LDA method is shown in Fig. 5(a). It can be found that the stopping power decreases as sample temperature increases, which show the same trends as the results obtained by the eFF simulations. This result further proves the effectiveness of the eFF method to calculate the stopping power of warm dense plasma, and on the other hand, it also shows that the electronic structure has a very important influence on the stopping power of warm dense plasma.

Comparing Figs. 4 and 5, it can be found that another obvious difference between the stopping power curves of eFF and the predictions of the theoretical models is that the stopping power curves obtained by the theoretical models have greater decline slope. The main reason for this difference is that the wave packet sizes of the projectile electrons in eFF simulations were constrained with its corresponding de Broglie wavelength, as mentioned in the computational details. A larger projectile energy corresponds to a smaller de Broglie wavelength, so the wave packet sizes of projectile electrons is also smaller. According to the interaction formula Eq. (10), a smaller projectile electron wave packet size will enhance the interaction between the projectile electron and the target electron, which has a positive effect on the improvement of the stopping power and leads to a decrease in the slope of the stopping power curve.

Different from the description in the eFF method, the projectile electrons are treated as classical point-charged particles in the previous theoretical models, and the quantum wave effect is not considered. Therefore, a different slope of the stopping power curve is obtained by these theoretical models. This difference between simulation and theoretical results reminds us that the quantum effect of projectile electrons will have a impact on the stopping power, especially when the de Broglie wavelength of the projectile electrons is close to the Wigner-Seitz radius of the target, e.g., the stopping of low-speed electrons in high-density target. For WDM, the quantum effect of projectile electrons may have an important influence on the stopping power and needs to be considered in the construction of a more sophisticated theoretical model.

We have investigated the stopping power models for solid targets through a large amount of literature. Although the influence of bound state is considered, these models usually do not consider the influence of target temperature on stopping power [78], such as SRIM [79], Casp [80], etc. Therefore, there are also limitations in calculating the stopping power of warm dense plasmas. In addition, according to our investigation and the introduction of related review article [78], only a small number of codes for these theoretical models are available on the internet, such as SRIM and Casp. Meanwhile, these models can only calculate the stopping power of target on the ion beam, so they are not suitable for the problem considered in this work.

IV. CONCLUSION

Different from the hot plasma state and the cold condensed state, a unified approximate model to simplify the properties of the warm dense state is still in the early stages [81], which makes the research on the stopping power of the warm dense plasma full of challenges. In this work, the stopping power of warm dense hydrogen for electron is studied using eFF method, which could take the dynamic effects of electronic structure into consideration and avoid the Coulomb catastrophe in the classical Coulomb system, so that the stopping power contributed by both ions and electrons in the sample can be considered at the same time. It is found from the eFF simulations that the stopping power of warm dense hydrogen decrease as the sample temperature increases, which is contrary to the prediction of various theoretical models

extensively used for weak-coupling plasmas. Further analysis and the calculation results of the LDA method prove that the reason for this difference is that the change of the electronic structure at different temperatures has an important effect on the stopping power of warm dense hydrogen, which is not considered in the previous theoretical models. In addition, the existence of molecular structure under low-temperature conditions increases the effective mass of target electrons during the collision process, which in turn leads to a decrease in energy transfer during the collision process. The effect of molecular structure and electronic structure form a competitive relationship, resulting in insensitivity of stopping power to temperature changes in the low-temperature range. In the fast-ignition scheme of ICF, if our goal is to deposit more energy in the warm dense fuel, our results will lead to a disappointing prediction, since the temperature rise of the fusion fuel caused by the deposition of electron energy will in turn reduce the efficiency of energy deposition.

The situation considered in this work is the stopping process of single electron in WDM, rather than that of coherent electron beams. There will be more complex phenomena in the stopping power of the electron beam, such as return currents, self-generated magnetic fields, and various instabilities [21,24]. Considering the electron stopping in a more practical case such as fast ignition of ICF, the collective effect of the electron beam will lead to a significant difference in the energy transport process compared to the situation of single electron, which should be considered in a further investigation of stoping power of WDM on electrons.

APPENDIX A: STOPPING POWER TO PROJECTILE ELECTRONS WITH LOW ENERGY

Except for the cases of incident electrons with energies from 400–10000 eV, we have performed eFF simulations for the stopping power of warm dense hydrogen to electrons with initial energy range from 10–100 eV. Due to the large stopping power and small initial projectile energy, the penetration depth of incident electrons is very small and most of the electrons cannot penetrate the sample. Therefore, the method of calculating stopping power with Eq. (2) is no longer applicable. The average energy loss during the entire period when the projectile electron energy drops from the initial energy to zero
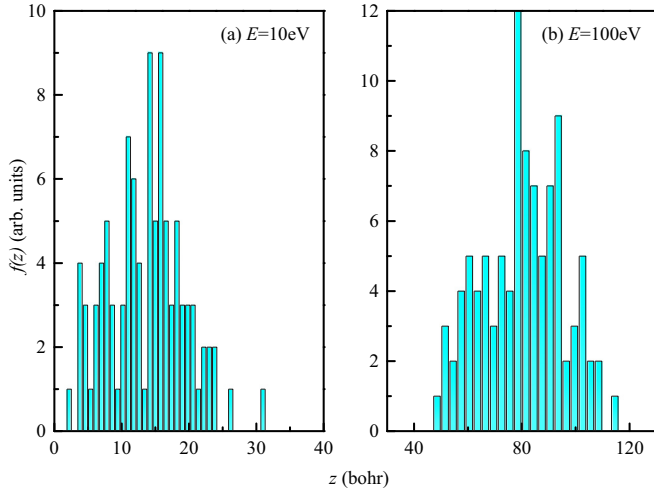
FIG. 7. The penetration depth distribution of projectile electrons $f(z)$. The target temperature is $T = 1$ eV. (a) and (b) correspond to the case whose projectile electron energy is 10 eV and 100 eV, respectively.

can be estimated from the penetration depth of the projectile particles as

$$-\overline{\frac{dE_i}{dx}} \approx \frac{E_0}{l_i}, \tag{A1}$$

where $-\overline{dE_i/dx}$ is the mean stopping power of the sample to a projectile electron with index i, E_0 and l_i are the initial energy the penetration depth of electron i. Figure 7 shows the penetration distribution of projectiles with incident energies of 10 eV and 100 eV in warm dense hydrogen at sample temperature $T = 1$ eV. The average stopping power calculated with Eq. (A1) to the incident electrons with initial energy of 10 eV and 100 eV is 350.3 MeV/cm and 484.5 MeV/cm, respectively. This result indicates that the stopping power has a maximum value in the range of the projectile energy from 10–400 eV, which is consistent with the previous experimental results in gaseous H_2 [41], although the thermodynamic state of the target is different. Therefore, both experiments and eFF simulations have confirmed that there is a Bragg peak structure similar to ions during the energy loss process of electrons in matter.

The stopping power for low-speed projectile electron at different target temperature is calculated with Eq. (A1) and listed in Table II. It shows that the stopping power in high-temperature target is much smaller than that in low-temperature target, which shows the same trend with the result

TABLE II. The stopping power calculated with Eq. (A1) for low-speed projectile electron in target at different temperature. E_p is the projectile energy, T is the target temperature, and $-dE/dx$ is the stopping power. The unit of stopping power $-dE/dx$ is MeV/cm.

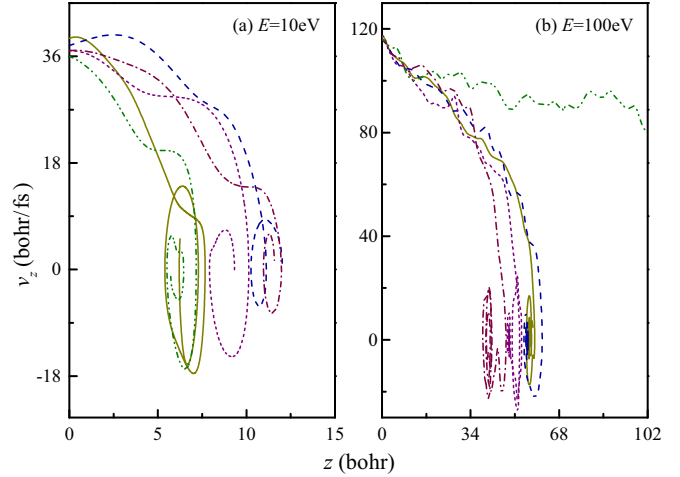| E_p(eV)/$-dE/dx$/T(eV)	0.1	0.4	1	2	4	10
10	840.3	748.9	350.3	324.8	209.4	154.6
100	414.4	463.0	484.5	487.0	335.8	244.5

FIG. 8. Phase diagram of several captured electrons. The target temperature is $T = 1$ eV. (a) and (b) correspond to the case whose projectile electron energy is 10 eV and 100eV, respectively.

obtained in the theoretical work of Archubi *et al.* [81], whose projectile particle is proton and target materials is Si, C, and Fe. The consistency of the trends is helpful to cross validate the effectiveness of the eFF method and the unified theoretical model proposed by Archubi *et al.*

In addition, it can be found from Table II that for low-temperature target (0.1 eV and 0.4 eV), the stopping power of projectile electron with $E_0 = 10$ eV is higher than that with $E_0 = 100$ eV, while for high-temperature targets ($T \geqslant 1$ eV), the stopping power of faster projectile electron is lower. This comparison indicates that as the temperature of the target plasma increases, the Bragg peak of the stopping power on electron will shift to the direction of higher projectile energy.

In addition, five low-velocity projectile electrons are randomly selected in the simulations and the phase trajectory of these electrons in the warm dense hydrogen target are illustrated in Fig. 8. It can be seen that the phase trajectory shows an obvious characteristic of circular motion for these projectile electrons with low initial energy. The circular motion of projectile electrons indicates that the dominant mechanism of its motion is the Coulomb attraction field provided by the ions in the target. We can regard this phenomenon as the capture process of projectile electrons by target ions and the capture velocity could be estimated by the similar derivation process to solving the first cosmic velocity in astrophysics. In various theoretical models, since the mass of ions is much greater than that of electrons, the main contribution of stopping power always comes from electrons and the contribution of ions is negligible. However, this capture phenomenon in the low-velocity range indicates that the stopping power of ions will play a leading role in the low-velocity range.

APPENDIX B: COMPUTATIONAL DETAILS OF ELECTRON FORCE FIELD

The electron force field is a theoretical model based on a simplified solution to the time-dependent Schrödinger equation. In the eFF method, the electronic wave function of electrons is approximately described as spherical Gaussian

wave packets whose position $\mathbf{x}$ and size s vary over time:

$$\Psi(\mathbf{r}) \propto \prod_j \exp\left\{-\left[\frac{1}{s^2} - \frac{2p_s}{s}\frac{i}{\hbar}\right](\mathbf{r}-\mathbf{x})^2 - \frac{i}{\hbar}\mathbf{p_x}\cdot\mathbf{r}\right\},$$

(B1)

where $\mathbf{p_x}$ and p_s is the conjugate momentum of $\mathbf{x}$ and s. The semiclassical Hamilton equations of motion for $\mathbf{x}$ and s are derived [82] by substituting the wave packet form into the time-dependent Schrödinger equation, which leads to

$$\dot{\mathbf{p}}_\mathbf{x} = -\nabla_\mathbf{x} V, \qquad \mathbf{p_x} = m_e \dot{\mathbf{x}},$$
$$\dot{p}_s = -\frac{\partial V}{\partial s}, \qquad p_s = \frac{3}{4}m_e\dot{s},$$

(B2)

with $V = V_{ii} + V_{ie} + V_{ee} + E_{KE} + E_{\text{Pauli}}$. The time derivatives are denoted as dots overhead in Eq. (B2). Here, V_{ii}, V_{ee}, and V_{ie} represent the screened electrostatic interactions between all pairs of ion-ion, electron-electron, and ion-electron, respectively. E_{KE} and E_{Pauli} are the electronic kinetic energy of the Gaussian wave packet and Pauli repulsion energy, which account for quantum mechanical effects of electrons. Each type of energy term can be expressed by the following expressions:

$$E_{KE} = \frac{1}{2}\sum_i \int |\nabla\psi_i|^2 dV = \sum_i \frac{3}{2}\frac{1}{s_i^2}$$

$$V_{ii} = \sum_{i<j} \frac{Z_i Z_j}{R_{ij}}$$

$$V_{ie} = -\sum_{i,j} Z_i \int \frac{|\psi_j|^2}{R_{ij}} dV = -\sum_{i,j} \frac{Z_i}{R_{ij}} \text{Erf}\left(\frac{\sqrt{2}R_{ij}}{s_i}\right)$$

$$V_{ee} = \sum_{i<j} \int \frac{|\psi_i|^2|\psi_j|^2}{x_{ij}} dV = \sum_{i<j} \frac{1}{x_{ij}} \text{Erf}\left(\frac{\sqrt{2}x_{ij}}{\sqrt{s_i^2+s_j^2}}\right)$$

$$E_{\text{Pauli}} = \sum_{\sigma_i=\sigma_j} E(\uparrow\uparrow)_{ij} + \sum_{\sigma_i\neq\sigma_j} E(\uparrow\downarrow)_{ij}$$

where σ denoting the spin of the electrons, $\text{Erf}(x)$ is the error function, which is defined as $\text{Erf}(x) = \frac{2}{\sqrt{\pi}}\int_0^x e^{-u^2}du$. $E(\uparrow\uparrow)$ and $E(\uparrow\downarrow)$ are the Pauli potential functions:

$$E(\uparrow\uparrow)_{ij} = \left(\frac{S_{ij}^2}{1-S_{ij}^2} + (1-\rho)\frac{S_{ij}^2}{1+S_{ij}^2}\right)\Delta T_{ij}$$

$$E(\uparrow\downarrow)_{ij} = \frac{\rho S_{ij}^2}{1+S_{ij}^2}\Delta T_{ij},$$

where ΔT is a measure of the kinetic energy change upon antisymmetrization, and S is the overlap between two wave packets:

$$\Delta T_{ij} = \frac{3}{2}\left(\frac{1}{\bar{s}_i^2} + \frac{1}{\bar{s}_j^2}\right) - \frac{2\left[3(\bar{s}_i^2+\bar{s}_j^2) - 2\bar{x}_{ij}^2\right]}{(\bar{s}_i^2+\bar{s}_j^2)^2}$$

$$S_{ij} = \left(\frac{2}{\bar{s}_i/\bar{s}_j + \bar{s}_j/\bar{s}_i}\right)^{3/2}\exp\left(-\frac{\bar{x}_{ij}^2}{\bar{s}_i^2+\bar{s}_j^2}\right),$$

where $\rho = -0.2$, $\bar{x}_{ij} = 1.125x_{ij}$, and $\bar{s}_i = 0.9s_i$.

The specific form chosen for Pauli potential distinguishes eFF from methods such as wave packet molecular dynamics, which can not produce stable molecule structure and can not describe the EOS of dense hydrogen accurately. The three universal parameters in the Pauli potential function are obtained through optimization. For more theoretical and technical details about the eFF method, please refer to Ref. [83].

[1] E. Fourkal, B. Shahine, M. Ding, J. S. Li, T. Tajima, and C.-M. Ma, Med. Phys. **29**, 2788 (2002).

[2] C. Zeitlin, Health Phys. **103**, 540 (2012).

[3] H. Nikjoo, S. Uehara, D. Emfietzoglou, and A. Brahme, New J. Phys. **10**, 075006 (2008).

[4] J. W. Wilson, F. A. Cucinotta, J. Miller, J. L. Shinn, S. A. Thibeault, R. C. Singleterry, L. C. Simonsen, and M. H. Kim, MRS Proc. **551**, 3 (1998).

[5] L. Campbell and M. J. Brunger, Int. Rev. Phys. Chem. **35**, 297 (2016).

[6] C. Bertulani, Phys. Lett. B **585**, 35 (2004).

[7] G. Hanel, B. Gstir, S. Denifl, P. Scheier, M. Probst, B. Farizon, M. Farizon, E. Illenberger, and T. D. Märk, Phys. Rev. Lett. **90**, 188104 (2003).

[8] F. Blanco, A. Muñoz, D. Almeida, F. Ferreira da Silva, P. Limão Vieira, M. C. Fuss, A. G. Sanz, and G. García, Eur. Phys. J. D **67**, 199 (2013).

[9] M. A. Huels, B. Boudaïffa, P. Cloutier, D. Hunting, and L. Sanche, J. Amer. Chem. Soc. **125**, 4467 (2003).

[10] M. Tabak, J. Hammer, M. E. Glinsky, W. L. Kruer, S. C. Wilks, J. Woodworth, E. M. Campbell, M. D. Perry, and R. J. Mason, Phys. Plasmas **1**, 1626 (1994).

[11] R. Betti and O. A. Hurricane, Nature Phys. **12**, 435 (2016).

[12] S. Atzeni and J. Meyer-ter Vehn, *The Physics of Inertial Fusion: Beamplasma Interaction, Hydrodynamics, Hot Dense Matter* (Oxford University Press, Oxford, 2004).

[13] C. Deutsch, H. Furukawa, K. Mima, M. Murakami, and K. Nishihara, Phys. Rev. Lett. **77**, 2483 (1996).

[14] E. R. Harrison, Phys. Rev. Lett. **11**, 535 (1963).

[15] M. Bailly-Grandvaux, J. J. Santos, C. Bellei, P. Forestier-Colleoni, S. Fujioka, L. Giuffrida, J. J. Honrubia, D. Batani, R. Bouillaud, M. Chevrot, J. E. Cross, R. Crowston, S. Dorard, J.-L. Dubois, M. Ehret, G. Gregori, S. Hulin, S. Kojima, E. Loyez, J.-R. Marquès *et al.*, Nature Commun. **9**, 102 (2018).

[16] A. Caruso and V. A. Pais, Nucl. Fusion **36**, 745 (1996).

[17] M. Murakami, H. Nagatomo, H. Azechi, F. Ogando, M. Perlado, and S. Eliezer, Nucl. Fusion **46**, 99 (2005).

[18] H. Nagatomo, T. Johzaki, T. Asahina, M. Hata, Y. Sentoku, K. Mima, and H. Sakagami, Nucl. Fusion **59**, 106055 (2019).

[19] S. Atzeni and M. Tabak, Plasma Phys. Controlled Fusion **47**, B769 (2005).

[20] T. Johzaki, M. Hino, M. Horio, S. Takeda, W. Kim, T. Endo, S. Fujioka, Y. Sentoku, H. Nagatomo, and A. Sunahara, High Energy Density Phys. **36**, 100841 (2020).

[21] A. Okabayashi, H. Habara, T. Yabuuchi, T. Iwawaki, and K. A. Tanaka, Phys. Plasmas **20**, 083301 (2013).

[22] C. K. Li and R. D. Petrasso, Phys. Rev. E **73**, 016402 (2006).

[23] C. K. Li and R. D. Petrasso, Phys. Rev. E **70**, 067401 (2004).

[24] Y. Sentoku, K. Mima, P. Kaw, and K. Nishikawa, Phys. Rev. Lett. **90**, 155001 (2003).

[25] L. D. Landau, Phys. Z. Sowjetunion **10**, 154 (1936).

[26] L. Spitzer Jr, Am. J. Phys. **31**, 890 (1963).

[27] Z. G. Fu, Z. G. Wang, and P. Zhang, Phys. Plasmas **24**, 112710 (2017).

[28] M. W. C. Dharma-wardana, Phys. Rev. Lett. **101**, 035002 (2008).

[29] M. D. Barriga-Carrasco, Phys. Rev. E **79**, 027401 (2009).

[30] L. S. Brown, D. L. Preston, and R. L. Singleton Jr., Phys. Rep. **410**, 237 (2005).

[31] D. Ward, H. R. Andrews, I. V. Mitchell, W. N. Lennard, R. B. Walker, and N. Rud, Can. J. Phys. **57**, 645 (1979).

[32] H. Geissel, H. Weick, C. Scheidenberger, R. Bimbot, and D. Gardèas, Nucl. Instrum. Methods Phys. Res., Sect. B **195**, 3 (2002).

[33] A. Mertens and H. Winter, Phys. Rev. Lett. **85**, 2825 (2000).

[34] A. B. Zylstra, J. A. Frenje, P. E. Grabowski, C. K. Li, G. W. Collins, P. Fitzsimmons, S. Glenzer, F. Graziani, S. B. Hansen, S. X. Hu, M. G. Johnson, P. Keiter, H. Reynolds, J. R. Rygg, F. H. Séguin, and R. D. Petrasso, Phys. Rev. Lett. **114**, 215002 (2015).

[35] J. A. Frenje, P. E. Grabowski, C. K. Li, F. H. Séguin, A. B. Zylstra, M. Gatu Johnson, R. D. Petrasso, V. Y. Glebov, and T. C. Sangster, Phys. Rev. Lett. **115**, 205001 (2015).

[36] A. Frank, A. Blažević, V. Bagnoud, M. M. Basko, M. Börner, W. Cayzac, D. Kraus, T. Heßling, D. H. H. Hoffmann, A. Ortner, A. Otten, A. Pelka, D. Pepler, D. Schumacher, A. Tauschwitz, and M. Roth, Phys. Rev. Lett. **110**, 115001 (2013).

[37] D. H. H. Hoffmann, K. Weyrich, H. Wahl, D. Gardés, R. Bimbot, and C. Fleurier, Phys. Rev. A **42**, 2313 (1990).

[38] A. Frank, A. Blažević, P. L. Grande, K. Harres, T. Heßling, D. H. H. Hoffmann, R. Knobloch-Maas, P. G. Kuznetsov, F. Nürnberg, A. Pelka, G. Schaumann, G. Schiwietz, A. Schökel, M. Schollmeier, D. Schumacher, J. Schütrumpf, V. V. Vatulin, O. A. Vinokurov, and M. Roth, Phys. Rev. E **81**, 026401 (2010).

[39] W. Cayzac, A. Frank, A. Ortner, V. Bagnoud, M. M. Basko, S. Bedacht, C. Bläser, A. Blažević, S. Busold, O. Deppert, J. Ding, M. Ehret, P. Fiala, S. Frydrych, D. O. Gericke, L. Hallo, J. Helfrich, D. Jahn, E. Kjartansson, A. Knetsch *et al.*, Nature Commun. **8**, 15693 (2017).

[40] M. Zawadzki and M. A. Khakoo, Phys. Rev. A **99**, 042703 (2019).

[41] A. Muñoz, J. C. Oller, F. Blanco, J. D. Gorfinkiel, and G. García, Chem. Phys. Lett. **433**, 253 (2007).

[42] S. Zhao, W. Kang, J. Xue, X. Zhang, and P. Zhang, J. Phys. Cond. Matter **27**, 025401 (2014).

[43] Y. H. Ding, A. J. White, S. X. Hu, O. Certik, and L. A. Collins, Phys. Rev. Lett. **121**, 145001 (2018).

[44] J. M. Pruneda, D. Sánchez-Portal, A. Arnau, J. I. Juaristi, and E. Artacho, Phys. Rev. Lett. **99**, 235501 (2007).

[45] V. U. Nazarov, J. M. Pitarke, Y. Takada, G. Vignale, and Y. C. Chang, Int. J. Mod. Phys. B **22**, 3813 (2008).

[46] M. Quijada, A. G. Borisov, I. Nagy, R. Diez Muiño, and P. M. Echenique, Phys. Rev. A **75**, 042902 (2007).

[47] A. J. White, O. Certik, Y. H. Ding, S. X. Hu, and L. A. Collins, Phys. Rev. B **98**, 144302 (2018).

[48] R. J. Magyar, L. Shulenburger, and A. D. Baczewski, Contrib. Plasma Phys. **56**, 459 (2016).

[49] E. S. Evans, S. A. Cohen, and D. R. Welch, Phys. Plasmas **25**, 042105 (2018).

[50] J. Kim, B. Qiao, C. McGuffey, M. S. Wei, P. E. Grabowski, and F. N. Beg, Phys. Rev. Lett. **115**, 054801 (2015).

[51] Z. Donkó, J. Phys. A: Math. Theor. **42**, 214029 (2009).

[52] P. E. Grabowski, M. P. Surh, D. F. Richards, F. R. Graziani, and M. S. Murillo, Phys. Rev. Lett. **111**, 215002 (2013).

[53] G. Dimonte and J. Daligault, Phys. Rev. Lett. **101**, 135001 (2008).

[54] C. Gao, S. Zhang, W. Kang, C. Wang, P. Zhang, and X. T. He, Phys. Rev. B **94**, 205115 (2016).

[55] B. Z. Chen, D. Wu, J. R. Ren, D. H. H. Hoffmann, and Y. T. Zhao, Phys. Rev. E **101**, 051203(R) (2020).

[56] D. Wu, X. T. He, W. Yu, and S. Fritzsche, Phys. Rev. E **95**, 023207 (2017).

[57] J. R. Ren, Z. G. Deng, W. Qi, B. Z. Chen, B. B. Ma, X. Wang, S. Yin, J. H. Feng, W. Liu, Z. F. Xu, D. H. H. Hoffmann, S. Y. Wang, Q. P. Fan, B. Cui, S. K. He, Z. R. Cao, Z. Q. Zhao, L. F. Cao, Y. Q. Gu, S. P. Zhu *et al.*, Nature Commun. **11**, 5157 (2020).

[58] G. Zwicknagel, C. Toepffer, and P.-G. Reinhard, Hyperfine Interact. **99**, 285 (1996).

[59] Y. Yao, Q. Zeng, K. Chen, D. Kang, Y. Hou, Q. Ma, and J. Dai, Phys. Plasmas **28**, 012704 (2021).

[60] D. Klakow, C. Toepffer, and P. Reinhard, J. Chem. Phys. **101**, 10766 (1994).

[61] P. E. Grabowski, *Frontiers and Challenges in Warm Dense Matter* (Springer International Publishing, Cham, 2014), Chap. A Review of Wave Packet Molecular Dynamics, pp. 265–282.

[62] J. T. Su and W. A. Goddard III, J. Chem. Phys. **131**, 244501 (2009).

[63] J. T. Su and W. A. Goddard, Proc. Natl. Acad. Sci. **106**, 1001 (2009).

[64] A. Jaramillo-Botero, J. Su, A. Qi, and W. A. Goddard, J. Comput. Phys. **32**, 497 (2011).

[65] P. L. Theofanis, A. Jaramillo-Botero, W. A. Goddard III, and H. Xiao, Phys. Rev. Lett. **108**, 045501 (2012).

[66] Q. Ma, J. Y. Dai, D. D. Kang, M. S. Murillo, Y. Hou, Z. X. Zhao, and J. M. Yuan, Phys. Rev. Lett. **122**, 015001 (2019).

[67] S. Plimpton, J. Comput. Phys. **117**, 1 (1995).

[68] Q. Ma, J. Dai, D. Kang, M. S. Murillo, Y. Hou, Z. Zhao, and J. Yuan, Phys. Rev. Lett. **123**, 099901(E) (2019).

[69] M. Bonitz, T. Dornheim, Z. A. Moldabekov, S. Zhang, P. Hamann, H. Kählert, A. Filinov, K. Ramakrishna, and J. Vorberger, Phys. Plasmas **27**, 042710 (2020).

[70] M. S. Murillo, Phys. Rev. E **81**, 036403 (2010).

[71] J. Lindhard, Kg. Danske Videnskab. Selskab. Mat.-Fys. Medd **28** (1954).

[72] A. A. Shukri, F. Bruneval, and L. Reining, Phys. Rev. B **93**, 035128 (2016).

[73] S. Zhang, H. W. Wang, W. Kang, P. Zhang, and X. T. He, Phys. Plasmas **23**, 042707 (2016).

[74] P. Giannozzi, S. Baroni, N. Bonini, M. Calandra, R. Car, C. Cavazzoni, D. Ceresoli, G. L. Chiarotti, M. Cococcioni, I. Dabo, A. D. Corso, S. de Gironcoli, S. Fabris, G. Fratesi, R. Gebauer, U. Gerstmann, C. Gougoussis, A. Kokalj, M. Lazzeri,

L. Martin-Samos *et al.*, J. Phys.: Condens. Matter **21**, 395502 (2009).

[75] P. E. Blöchl, Phys. Rev. B **50**, 17953 (1994).

[76] J. P. Perdew, K. Burke, and M. Ernzerhof, Phys. Rev. Lett. **77**, 3865 (1996).

[77] L. González-Gallego, M. D. Barriga-Carrasco, and J. Vázquez-Moyano, Phys. Plasmas **28**, 043103 (2021).

[78] P. Sigmund and A. Schinner, Nucl. Instrum. Meth. Phys. Res. B **382**, 15 (2016), the 21st International workshop on Inelastic Ion Surface Collisions (IISC-21).

[79] J. F. Ziegler, M. D. Ziegler, and J. P. Biersack, Nucl. Instrum. Meth. Phys. Res. B **268**, 1818 (2010).

[80] G. Schiwietz and P. Grande, Nucl. Instrum. Meth. Phys. Res. B **153**, 1 (1999).

[81] C. D. Archubi and N. R. Arista, Phys. Rev. A **102**, 052811 (2020).

[82] E. J. Heller, J. Chem. Phys. **62**, 1544 (1975).

[83] J. T. Su, Ph.D. thesis, An electron force field for simulating large scale excited electron dynamics, California Institute of Technology, 2007.